The impacts of bias in cloud-radiation-dynamics interactions on central Pacific seasonal and El Niño simulations in contemporary GCMs

AGU PUBLICATIONS

Earth and Space Science

RESEARCH ARTICLE
10.1002/2017EA000304

Key Points:
- Current GCMs exclude snow-radiative effects
- Excluding snow-radiative effects leads to weakening surface wind stress and warming SSTs in seasonal variation and CP-El Nino
- Including snow-radiative effects largely reduces the model biases of CP-El Nino events

Supporting Information:
- Supporting Information S1

Correspondence to:
J.-L. F. Li,
jli@jpl.nasa.gov

Citation:
Li, J.-L. F., Suhas, E., Richardson, M., Lee, W.-L., Wang, Y.-H., Yu, J.-Y., … Shen, M.-H. (2018). The impacts of bias in cloud-radiation-dynamics interactions on central Pacific seasonal and El Niño simulations in contemporary GCMs. *Earth and Space Science*, *5*, 50–60. https://doi.org/10.1002/2017EA000304

Received 26 MAY 2017
Accepted 23 DEC 2017
Accepted article online 11 JAN 2018
Published online 4 FEB 2018

The Impacts of Bias in Cloud-Radiation-Dynamics Interactions on Central Pacific Seasonal and El Niño Simulations in Contemporary GCMs

J.-L. F. Li[1], E. Suhas[1], Mark Richardson[1], Wei-Liang Lee[2], Yi-Hui Wang[1], Jia-Yuh Yu[3], Tong Lee[1], Eric Fetzer[1], Graeme Stephens[1], and Min-Hua Shen[3]

[1]Jet Propulsion Laboratory, California Institute of Technology, Pasadena, CA, USA, [2]RCEC, Academia Sinica, Taipei, Taiwan, [3]Department of Atmospheric Sciences, National Central University, Taoyuan City, Taiwan

Abstract Most of the global climate models (GCMs) in the Coupled Model Intercomparison Project, phase 5 do not include precipitating ice (aka falling snow) in their radiation calculations. We examine the importance of the radiative effects of precipitating ice on simulated surface wind stress and sea surface temperatures (SSTs) in terms of seasonal variation and in the evolution of central Pacific El Niño (CP-El Niño) events. Using controlled simulations with the CESM1 model, we show that the exclusion of precipitating ice radiative effects generates a persistent excessive upper-level radiative cooling and an increasingly unstable atmosphere over convective regions such as the western Pacific and tropical convergence zones. The invigorated convection leads to persistent anomalous low-level outflows which weaken the easterly trade winds, reducing upper-ocean mixing and leading to a positive SST bias in the model mean state. In CP-El Niño events, this means that outflow from the modeled convection in the central Pacific reduces winds to the east, allowing unrealistic eastward propagation of warm SST anomalies following the peak in CP-El Niño activity. Including the radiative effects of precipitating ice reduces these model biases and improves the simulated life cycle of the CP-El Niño. Improved simulations of present-day tropical seasonal variations and CP-El Niño events would increase the confidence in simulating their future behavior.

Plain Language Summary Despite considerable progress, coupled GCMs are still far from accurately representing tropical Pacific El Niño–Southern Oscillation events, mainly due to the involvement of complex air-sea interactions and sophisticated atmospheric and oceanic processes. In this study, we have identified the exclusion of atmospheric precipitating large-particle ice (also known as falling snow) radiative effects, as in most global climate models do not represent this effect, as an important factor. Our results suggest that the inclusion of the contribution of the precipitating ice and its radiative effects in models is important to improve the simulation of the Pacific mean state, seasonal cycle, and CP-El Niño.

1. Introduction

The tropical Pacific El Niño–Southern Oscillation (ENSO) is an internal climate fluctuation with worldwide impacts on weather and climate (e.g., McPhaden et al., 2006) whose warm phase is referred to as El Niño and cold phase as La Niña. Physical processes shaping ENSO structures have been widely discussed (e.g., Ashok et al., 2007; Kao & Yu, 2009; Kug et al., 2009; Larkin & Harrison, 2005; Trenberth & Stepaniak, 2001; Wang & Weisberg, 2000; Yu & Kao, 2007), and the warm-phase El Niño events are often categorized into two major types based on their spatial characteristics of sea surface temperature (SST) anomalies (Ashok et al., 2007; Kao & Yu, 2009; Kug et al., 2009; Larkin & Harrison, 2005; Yu & Kao, 2007). One, with SST warming mainly occurring over the cold tongue region, is defined as the eastern Pacific El Niño (EP-El Niño) and the other, with SST warming mainly centered over the central-equatorial Pacific, is defined as the central Pacific El Niño (CP-El Niño). EP-El Niño events evolve with the propagation or basin-wide fluctuation of upper-ocean temperature anomalies at the thermocline and are more associated with oceanic processes such as vertical advection and mixing/entrainment associated with large-scale air-sea interaction and feedback (Bjerknes feedback). Meanwhile CP-El Niño events have subsurface temperature anomalies that develop locally in the central-equatorial Pacific (e.g., Kao & Yu, 2009; Yu et al., 2011; Yu & Kao, 2007). They depend on upper-ocean dynamics and are more associated with local air-sea interactions closely tied to atmospheric forcing (Kao & Yu, 2009). Therefore, the two different types of El Niño may be examined separately in

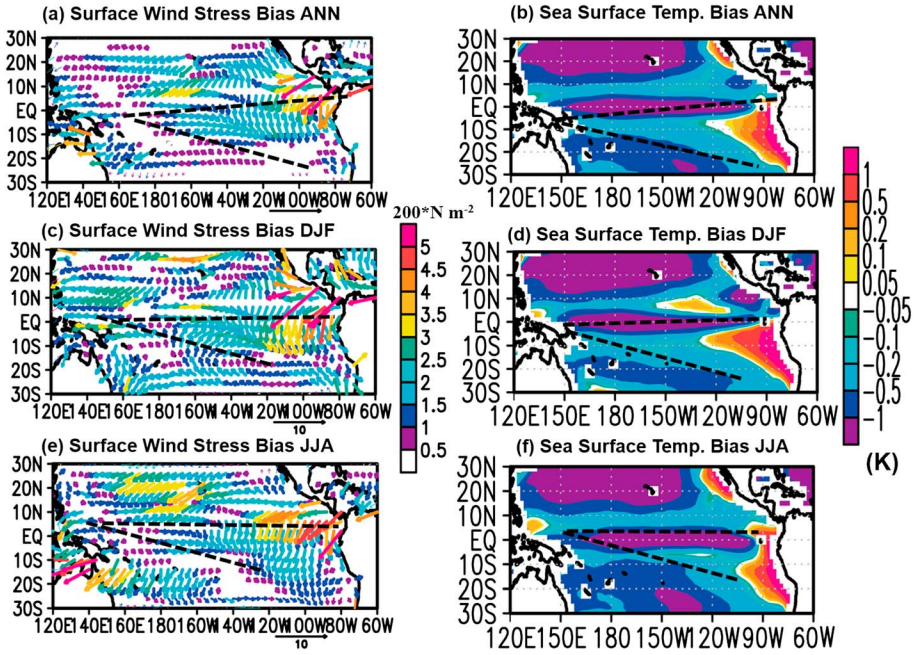

Figure 1. (a) Annual mean (ANN) CMIP5 models multimodel-mean surface wind stress minus QuikSCAT surface wind stress. (b) Same as Figure 1a but for sea surface temperatures minus extended reconstructed sea surface temperature (ERSST). (c, d) Same as Figures 1a and 1b but for December-January-February (DJF). (e, f) Same as Figures 1a and 1b but for June-July-August (JJA) for the CMIP5 GCMs listed in Table 1. The dashed lines delineate the main region where models tend to have weaker trade winds and warmer SSTs between the southern edge of the ITCZ (dashed line) and the northern edge of the SPCZ (dashed line), which we refer to as the V-shaped region.

global climate models (GCMs) such as the CMIP5 models used in the Intergovernmental Panel on Climate Change fifth Assessment Report (e.g., Kao & Yu, 2009; Kim et al., 2012; Yu & Kao, 2007).

Despite considerable progress, GCM biases in mean SSTs and surface wind stress remain large in the mean state (Lee et al., 2013; Li, Lee, Waliser, David Neelin, et al., 2014; Li, Lee, Waliser, Stachnik, et al., 2014), and in terms of seasonal variability and their evolution in El Niño events (e.g., Kao & Yu, 2009; Yu & Kao, 2007), leading to impacts on simulated climate variability (Guilyardi et al., 2009, Wittenberg, 2009). In general, coupled GCMs do not yet accurately represent El Niño events (Collins et al., 2010; Vecchi & Wittenberg, 2010).

The evolution of CP-El Niño events has been studied in observations (Ding et al., 2011; H.-M. Kim et al., 2009; Lee & McPhaden, 2010; Mo, 2010) and models in both CMIP3 (e.g., Meehl et al., 2007; Ham & Kug, 2011; Ham et al., 2012; Yu & Kim, 2010) and CMIP5 (e.g., Kim & Yu, 2012). Kim and Yu (2012), for example, found model differences in 21st century responses of CP-El Niño and EP-El Niño events to anthropogenic forcing.

This study aims at exploring and linking the potential impacts from the biases of mean states and seasonal variability of SSTs and wind stress on CP-El Niño evolution. (Li, Lee, Waliser, David Neelin, et al., 2014; Li, Lee, Waliser, Stachnik, et al., 2014; Li et al., 2016). These biases are linked to underestimated reflection of ice crystals in the air through a cloud-radiation-dynamics interaction mechanism proposed by Li, Lee, Waliser, David Neelin, et al. (2014) and Li et al. (2016) and shown in the supporting information (SI). Radiative impacts are shown in Figure S1, and the mechanism is schematically illustrated in Figure S2 and further explained in the rest of the paper.

Figure 1 shows biases in the CMIP5 annual mean (ANN), December-January-February (DJF) and June-July-August (JJA) surface wind stress against QuikSCAT (Figures 1a, 1c, and 1e) and sea surface temperature (SST) (Figures 1b, 1d, and 1f) versus the extended reconstruction SST record (Smith et al., 2008). Weaker trade winds and warmer SSTs are found between the southern edge of the Intertropical Convergence Zone (ITCZ) and the northern edge of the South Pacific Convergence Zone (SPCZ), which bound the flow and lead to low-level southeasterly convergence between them. We refer to this key area as the V-shaped region and focus on it as CMIP5 models agree on its general structure and location despite diversity in how they simulate the location and strength of the convergence zones. As Figure 1 shows an ensemble average, it smooths over

Table 1
List of CMIP5 Models Used, Those Shown With an Asterisk Do Not Include Snow Radiative Effects and So Were Used in Our Analysis

CMIP5 model name	Modeling center or group
*bcc-csm1	Beijing Climate Center
*CanESM2	Canadian Centre for Climate Modelling and Analysis
*CCSM4	National Center for Atmospheric Research
CESM1-CAM5	National Center for Atmospheric Research
*CNRM-CM5–2	Centre National de Recherches Météorologiques/ Centre Européen de Recherche et Formation Avancée en Calcul Scientifique
CSIRO-Mk3–6-0	Commonwealth Scientific and Industrial Research Organization in collaboration with Queensland Climate Change Centre of Excellence
*HadCEM2-CC	Met Office Hadley Centre
*HadCEM2-ES	Met Office Hadley Centre
HadCM3	Met Office Hadley Centre
*Inmcm4	Institute for Numerical Mathematics
*IPSL-CM5A-LR	Institut Pierre-Simon Laplace
*MPI-ESM-LR	
*MRI-CGCM3	Meteorological Research Institute
*MIROC5	Atmosphere and Ocean Research Institute (the University of Tokyo), National Institute for Environmental Studies, and Japan Agency for Marine-Earth Science and Technology
*NorESM1-M	Norwegian Climate Centre

these differences and so may tend to underestimate any individual model's bias. The biases in the V-shaped region are similar in CMIP3 (Li, Lee, Waliser, David Neelin, et al., 2014; Li, Lee, Waliser, Stachnik, et al., 2014; Li et al., 2015), and we propose that they are partly explained by the missing radiative effects of precipitating ice in most CMIP5 GCMs (see Table 1). Furthermore, it is natural to speculate that these biases will also affect the modeled seasonal variation and coupled atmosphere-ocean processes such as the CP-El Niño.

Biases associated with the exclusion of snow radiative effects are those expected from underestimated Ice water path (IWP) leading to changes in heating rate profiles, excessive downward shortwave (SW) at the surface shortwave downward radiative flux (RSDS), and upward longwave (LW) at top of atmosphere (TOA) Upward longwave radiative flux at the top of the atmosphere (RSUT) over deep convective regions (e.g., the ITCZ, western Pacific warm pool, and midlatitude storm tracks) (e.g., Li et al., 2013; Li, Lee, Waliser, David Neelin, et al., 2014; Li, Lee, Waliser, Stachnik, et al., 2014; see also Figure S4 for heating rate differences). We note that much high-altitude snow in the tropics occurs in stratiform clouds rather than convective towers, but these tropical stratiform clouds originate from mature convective structures (e.g., Houze, 1997), such that snow radiative effects occur within and near the convective regions.

Because of its close connection with atmospheric forcing, we propose that modeled CP-El Niño events are more likely to be affected by precipitating ice radiative effects than EP-El Niño. To test this proposed mechanism, we conduct simulations using the Community Earth System Model version 1 (CESM1) by turning on and off precipitating ice radiative calculations in its atmospheric component, the Community Atmosphere Model version 5 (CAM5). This is one of the few models that incorporates diagnostic snow and its effect on radiative fluxes, and this may be turned on or off as required (Gettelman et al., 2010; Li et al., 2012, 2013, 2015, 2016).

We explore the interlinks between SSTs, near-surface wind stress, and the trade winds in terms of the mean state, seasonal variability, and the life cycle of CP-El Niño events. We describe the methodology for determining CP-El Niño in section 2. In section 3, observational and model data are described. Results follow in section 4, and conclusions are drawn in section 5.

2. Methodology for Determining CP-El Niño

We extract the CP-El Niño signal in models and observations over 1900–2005 following the Kao and Yu (2009) SST-based methodology. First, we derive the monthly SST anomalies by subtracting the monthly climatology and the 1900–2005 linear trend, with the trend calculated separately for each grid point. To limit the influence from EP-El Niño, each grid cell's detrended anomalies are regressed against the detrended Niño1 + 2 SST anomalies. The regression coefficients are then used to produce a scaled Niño1 + 2 time series separately for each grid cell, and this scaled series is then removed from the grid cell monthly SST anomalies. Using empirical orthogonal function (EOF) analysis, we then obtain the resultant monthly SST anomalies. The first EOF represents the spatial pattern of CP-El Niño, and the first principle component (PC1) represents the time evolution of CP-El Niño events. An individual CP-El Niño event is identified based on the criterion that the normalized PC1 of SST exceeds a threshold value of 1 K for five consecutive months. We develop a composite CP-El Niño life cycle for a variety of variables by identifying and isolating 7 months before and 7 months after maximum in PC1 of the SST anomalies, summing up all individual CP-El Niño episodes, and dividing by the total number of CP-El Niño events. We identify 14 CP-El Niño events, of which 12 or 13 are also identified by two El Niño Modoki Index methods (Ashok et al., 2007; Li et al., 2010; see Table S1; Figure S3 shows that the disagreement in 1976/1977 occurs with an event that began with EP-El Niño features before propagating to CP-El Niño like). Given this agreement, we do not expect major biases to be introduced by selecting this EOF-based method to identify CP-El Niño events.

3. Data Sources

3.1. Observations and Reanalysis

The Energy Balanced and Filled Edition 2.6r version of Clouds and the Earth's Radiant Energy System (CERES) TOA radiative fluxes is used for SW and LW radiation fields (CERES_EBAF-TOA) (Loeb et al., 2009, 2012). Differences with the most recent Edition 4.0 are minor in the Pacific, peaking at less than 2 W m^{-2} compared with model-observation discrepancies commonly greater than 15 W m^{-2} (Figure S5). The extended reconstructed sea surface temperature (ERSST) analysis v3b (Smith et al., 2008) is used for SSTs over 1900–2005. ERSST is a global monthly sea surface temperature data set derived from the International Comprehensive Ocean–Atmosphere Dataset that uses advanced statistical techniques to infill and provide complete ocean coverage since January 1854.

The surface wind stress data are from measurements derived from the SeaWinds scatterometer on board the NASA QuickSCAT mission (Risien & Chelton, 2008) that sampled 90% of the global ocean each day from 1999 to 2009. The data set is available at http://cioss.coas.oregonstate.edu/scow/.

For dynamical fields we use the European Centre for Medium-Range Forecasts (ECMWF) ERA-Interim reanalysis (Dee & Uppala, 2009). A common grid of 4° × 5° latitude-longitude is applied for all observed fields.

3.2. CMIP5 Model Output

For each of the CMIP5 models listed in Table 1, we use a single historical simulation over 1900–2005 (simulation r1i1p1 in CMIP5 nomenclature). All outputs were placed on the same 4° × 5° latitude-longitude grid as the observations.

3.3. Sensitivity Experiments and CESM1 Coupled GCM

We use the fully coupled CESM1 GCM whose code and documentation are available from http://www.cesm.ucar.edu/models/cesm1.0/. (Morrison & Gettelman, 2008; Neale et al., 2012). The atmospheric component, the CAM5 includes macrophysics, deep and shallow cumulus convection, active aerosol formation, and a moist turbulence parameterization. In addition, the snow profile is diagnosed from falling mass ice flux profiles and interacts with radiation at each model level and time step (details can be found in Gettelman et al., 2010; Lindvall et al., 2013; Morrison & Gettelman, 2008). The simulated total ice and snow amounts are comparable to *CloudSat* retrieved products (Gettelman et al., 2008, 2010).

Two experiments are conducted following the CMIP5 historical protocol (Taylor et al., 2012) from 1850 to 2005: one from a control run with diagnostic cloud snow-radiation interaction on (hereafter, S) and another with the diagnostic snow-radiation effect off (hereafter, NoS). In both cases the snow is diagnosed, we only adjust whether it interacts with the radiation code. We then analyze the differences between the two experiments: snow-radiative effect off minus snow-radiative effect on (referred to as NoS-S) over 1900–2005 on the same 4° × 5° latitude-longitude grid used for observations.

4. Results

4.1. The Biases of Annual Mean Seasonal Surface Wind Stress and SSTs in CESM1 Sensitivity Experiments

Figure 2 shows the simulated CESM1 NoS-S changes in annual mean surface wind stress and SST over the Pacific for December-January-February (DJF) and June-July-August (JJA). Annual NoS-S changes are consistent with our expectations based on the mechanism proposed in Figure S2, particularly over the southern V-shaped region which is identified by bounded dashed lines. In addition, some of the features appear in the CMIP5 biases from Figure 1, where northwesterly anomalies oppose the mean trades and too-warm SSTs extend into the southern trade wind region. We also split the CMIP5 models into two subensembles representing the S and NoS models and considered the CMIP5 NoS-S SST differences in Figure S6. The CMIP5 NoS-S warm difference extends into the southern V-shaped region as in the CESM1 NoS-S comparison although there are other differences such as warmer SSTs in the coastal stratocumulus regions. The CMIP5 NoS-S comparison cannot isolate snow radiative effects as there are many other differences between CMIP5 S and NoS models. Nevertheless, the changes introduced in the southern V-shaped region in CESM1 by including snow radiative effects are similar to biases seen in the CMIP5 ensemble, and which are stronger in CMIP5-NoS models. This is suggestive that our proposed mechanism contributes to these

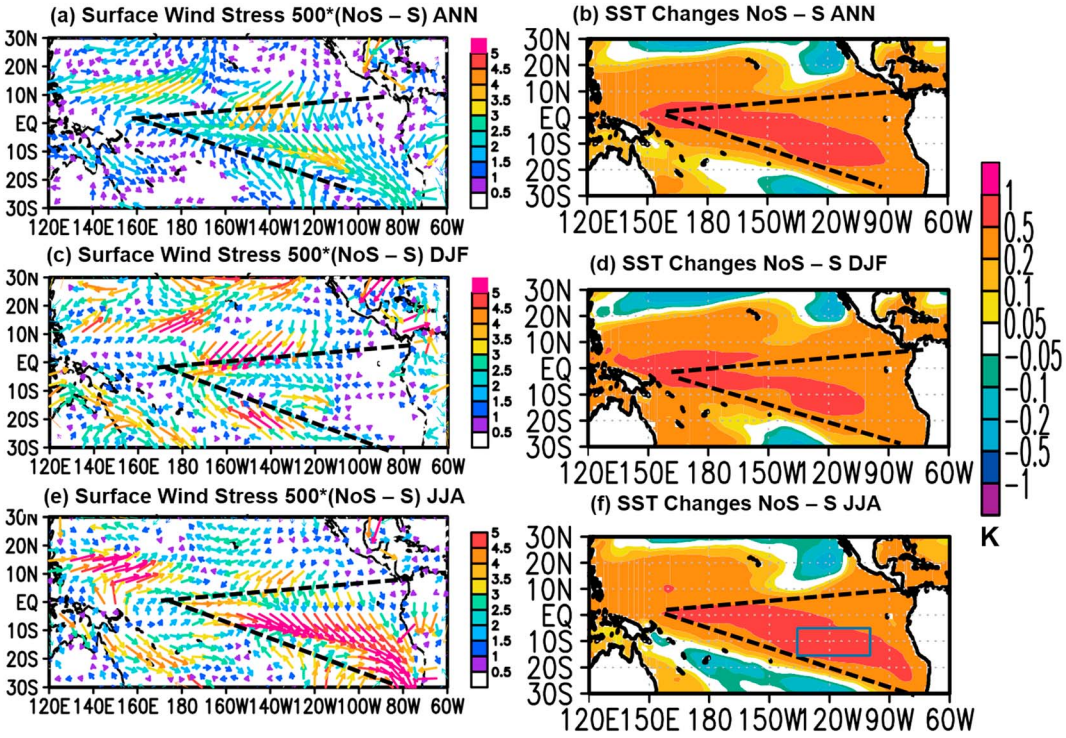

Figure 2. (a) CESM1 surface wind stress differences between snow-radiative effect off (NoS) and snow-radiative effect on (S), NoS-S, for annual mean (ANN). (b) Same as Figure 2a but for sea surface temperature (SST). (c, d) Same as Figures 2a and 2b but for December-January-February (DJF). (e, f) Same as Figures 2a and 2b but for June-July-August (JJA). Surface wind stress units: N m^{-2}. Dashed lines show the V-shaped region as described in Figure 1.

CMIP5 biases, although further controlled NoS-S experiments with other GCMs would be required to provide a robust estimate of its likely magnitude.

Within CESM1, we propose the following mechanism based on heating rate changes in convective regions (see Figure S4): excluding snow radiative effects leads to greater LW cooling at the highest altitudes (above about 250 hPa). This drives stronger updrafts from about 250–650 hPa and corresponding strengthening of

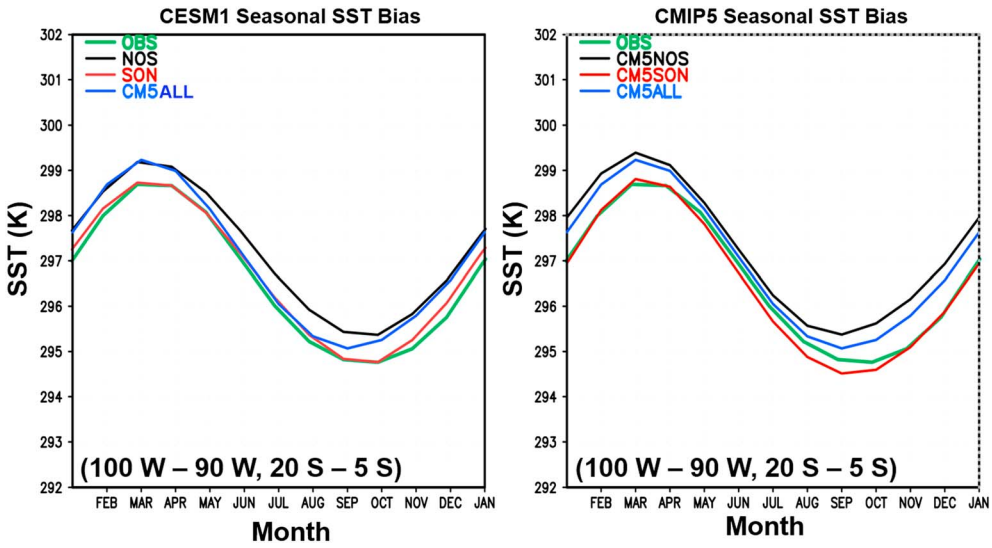

Figure 3. The (a) 1900–2005 mean seasonal cycle of sea surface temperature (SST) for CESM1 snow-radiative effect off (NOS: black line), snow-radiative effect on (SON: red line), multimodel mean for all CMIP5 models (CM5ALL: blue line), and ERSST SST (OBS: green line). (b) Same as Figure 3a but for the mean seasonal cycle of MMM from all CMIP5 models (CM5ALL: blue) and the ensemble CMIP5 model mean with considering snow-radiative effects (CM5NOS: black line) and the models with inclusion of snow-radiative effects (CM5SON: red line). All the lines are the average from a region in 100–90°W and 5–20°S.

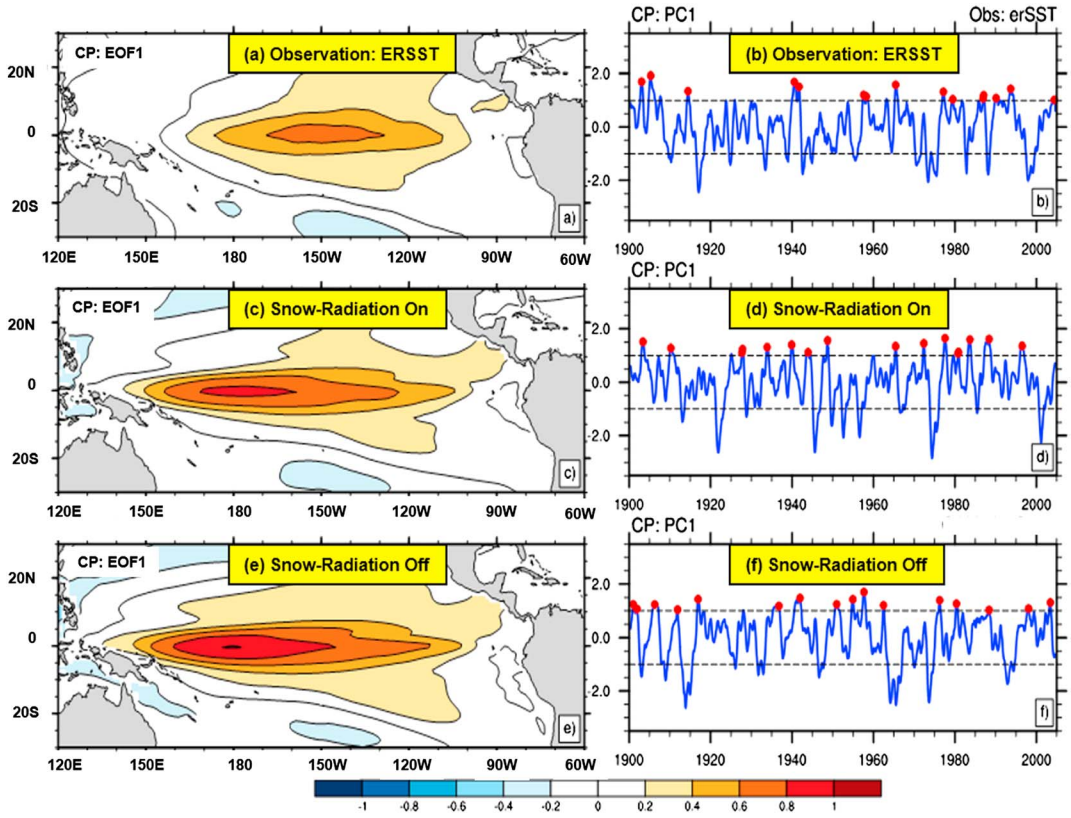

Figure 4. (a) First leading spatial EOF of SST anomaly (°C) and (b) corresponding principle component (PC) time series from ERSST (31.1% variance explained). (a) and (b) are derived from combined regression-EOF analysis for the central Pacific (CP) El Niño for 1900–2005. CP-El Niño events with normalized amplitude >1 are highlighted by red dots. (c, d) same as (a, b) but for CAM5 model with snow radiative effect (29.0% variance explained); (e, f) same as (c, d) but for CAM5 model without snow radiative effect (31.5% variance explained). See Table S2 for variance explained in a subset of other CMIP5 models.

downdrafts to the surface due to the requirements of the grid cell level cumulus parameterization. As a result, low-level moist and warm air originating from the warm pool and the ITCZ/SPCZ is advected northeastward and southeastward. As the southern Pacific high is more stable throughout the year (Li, Lee, Waliser, David Neelin, et al., 2014; Li, Lee, Waliser, Stachnik, et al., 2014), this manifests in the mean state as a clear and consistent bias in the southern Pacific V-shaped region with weaker surface wind stress and subsequent SST warming from reduced upper-ocean mixing.

Figure 3 compares the 1900–2005 mean annual cycle of the CMIP5 ensemble mean with the CESM1-NoS and CESM1-S and observed SSTs for the southern Pacific trade wind region (100–90°W; 5–20°S). The CESM1-S case (S) simulation is closer to observed SSTs in all months than the CESM1-NoS case (NOS), and the CMIP5 all-model mean (CM5ALL). CESM-NoS is consistently biased warm by about 1 K, while the CMIP5 bias shrinks from 1 K over October–April down to within 0.5 K in May–August. Figure 3b shows that CMIP5 models without snow radiative effects (CM5NOS) feature similar bias to CEMS1NoS, while CMIP5 models with snow radiative effects (CMIP5SON) show results similar to observations and the CESM1-S case.

4.2. CP-El Niño

Li, Lee, Waliser, Stachnik, et al. (2014) found that differences in upper-ocean temperature with and without snow radiative effects are consistent with expectations from the different strengths of vertical mixing due to ocean surface wind stress and cannot be explained by differences in net air-sea heat fluxes. In the tropics, we expect the largest direct radiative effects of snow to occur in clouds associated with convective activity, including the stratiform clouds linked to mature convective cores. Therefore, processes involving changes in the location and intensity of convection may be affected by excluding the radiative effects of falling snow. We focus on CP-El Niño rather than EP-El Niño as it is more strongly coupled to the atmosphere and so radiative adjustments should affect it more.

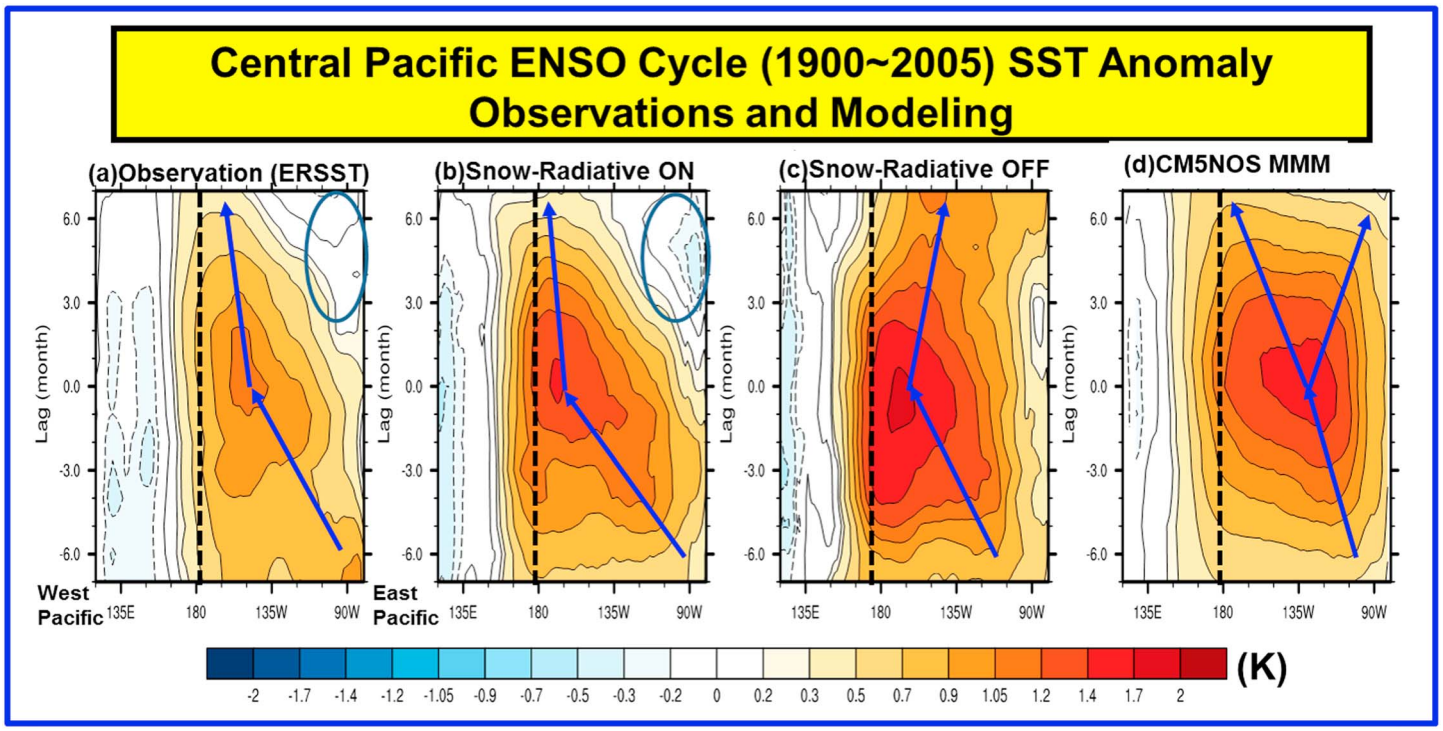

Figure 5. Life cycle composite of sea surface temperature (SST) anomalies (°C) associated with Central Pacific El Niño (CP-El Niño) averaged along the equatorial region (5°S–5°N) for (a) observations (ERSST), (b) NCAR CESM1 model with precipitating ice (snow) radiative effect, (c) NCAR CESM1 model without snow radiative effect, and (d) ensemble mean of all CMIP5 models that exclude falling snow radiative effects (CM5NOS-MMM). *Y* axis: −7 months to +7 months.

Figure 4 shows the leading EOF of SST anomalies (°C) in the mean warm phase and the corresponding principle component (PC) time series of CP-El Niño over 1900–2005 in ERSST observations (Figures 4a and 4b), CESM1-S (Figures 4c and 4d), and CESM1-NoS (Figures 4e and 4f). Warm phases of CP-El Niño, defined as normalized amplitude greater than 1, are highlighted by the red dots. In comparison with observations, warm-phase CP-El Niño model SST anomalies are warmer and farther to the west and NoS biases are larger than those in the S case. In fact, the mean state NoS-S SST differences are significantly different ($p < 0.05$) over the central ITCZ and trade wind regions in the central Pacific (Li, Lee, Waliser, David Neelin, et al., 2014), which must be explained in part by the CP-El Niño differences reported here.

Figure 5 contains SST anomaly Hovmöller diagrams of the composite CP-El Niño life cycle averaged near the equator (5°S–5°N) for observations, CESM1-S, CESM1-NoS, and CMIP5-NoS. Blue arrows show the warm-SST signal propagation from 6 months before the peak to 6 months after the peak. Both observed and modeled composite CP-El Niño events show an initial propagation of the warmth from the east (85°W) to near the central Pacific (150°W). Observations show that, historically, SST anomalies then decrease in magnitude and continue to propagate westward while the eastern Pacific cools. This SST cooling anomaly is indicated by a black oval and is also seen in the CESM1-S simulations, unlike in CESM1-NoS and the CMIP5-NoS mean, where there is a component that propagates eastward following the peak. This leads to late-cycle warm biases of 0.3–0.6 K relative to observations. Lower temperatures in the East Pacific is characteristic of CP-El Niño events, and the reduced CESM1-NoS biases here, while smaller than in the west, should affect atmospheric teleconnections and precipitation patterns and contribute to improved simulation of CP-El Niño-driven variability. We also present results for 15 CMIP5 models in Figure S7, which shows that the three CMIP5-S models (including CESM1-CAM5) tend to maintain warmer SSTs on the west, without propagating them eastward, whereas postpeak eastward propagation is common but not universal among CMIP5-NoS models. This indicates that our proposed mechanism may be more widespread among CMIP5 models, but it is not unique as an explanation to the eastward propagation discrepancy.

The anomalous surface wind stress (and 1,000 hPa winds) has been commonly used to explain the anomalous SST evolution for seasonal CP-El Niño activity. Unfortunately, the QuikSCAT surface wind data record

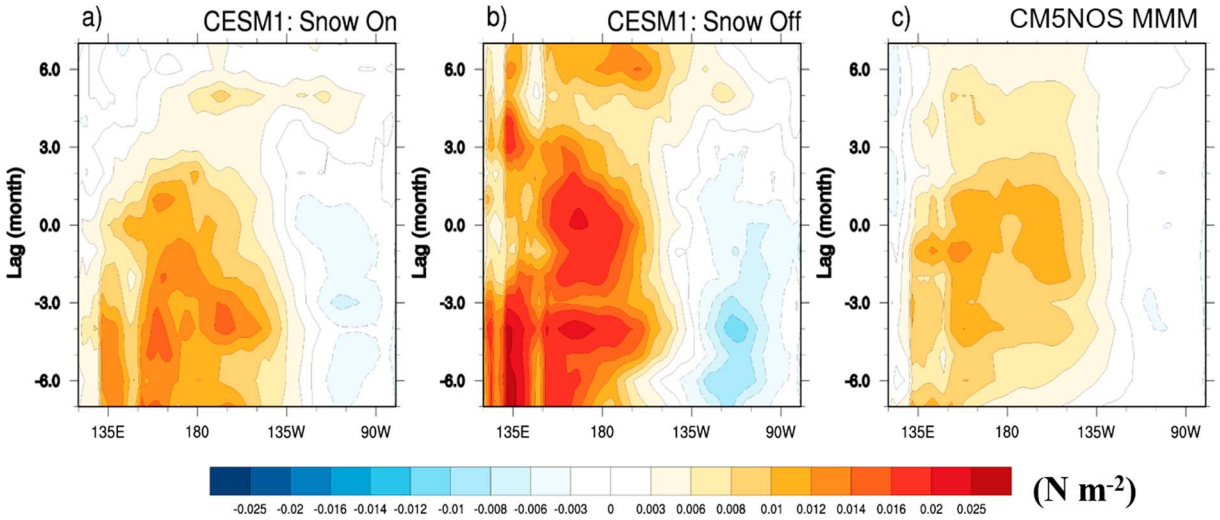

Figure 6. Life cycle composite of the zonal component of wind stress anomalies (N m^{-2}) associated with central Pacific El Niños averaged near the equator (5°S–5°N) for (a) CESM1 with snow radiative effect, (b) CESM1 without snow radiative effect, and (c) ensemble mean from all CMIP5 models without snow radiative effect (CM5NOS MMM).

is too short to capture sufficient events to produce a meaningful CP-El Niño composite, so we are only able to show model values in our wind stress Hovmöller diagrams in Figure 6. Figure 6a shows that in CESM1-S, anomalous surface westerly wind stress starts from the seventh month (lag −7) before the onset of CP-El Niño extending from the western Pacific (135°E) to near the dateline. The westerlies weaken after the peak (lag 0), associated with the weakened and more westerly CP-El Niño SST anomalies shown in Figure 3a. The CESM1-NoS case shows much stronger westerly surface wind stress anomaly (i.e., weakening total easterly surface wind stress) throughout the full life cycle without the obvious die-off after lag +3 months (Figure 6b). Wind stress magnitudes in the CMIP5-NoS multimodel mean are lower, partly as models place their CP-El Niño peaks at different longitudes (see Figure S7), and so their surface wind vectors cancel somewhat. However, the CMIP5-NoS ensemble show stronger continued wind stress after lag +3 months.

The above findings are consistent with Li et al. (2016) and with our hypothesized process by which the missing radiative effects of snow lead to increased surface outflow from convective regions, subsequently affecting surface wind stress elsewhere. Similar patterns of SSTs and surface wind stress imply that the damped easterly trades reduce upper-ocean vertical mixing as well as cold water advection in the oceanic mixed layer (Li et al., 2016), which in turn warm SSTs to the east, allowing longer-lasting CP-El Niño events in which the warm anomalies are also able to propagate eastward, at least in CESM1.

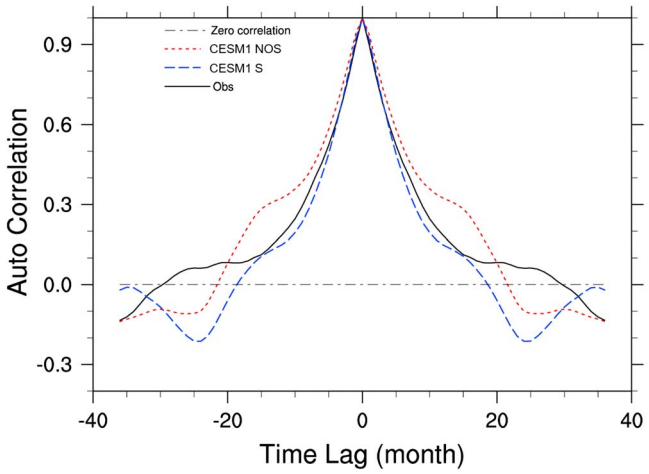

Figure 7. Lead-lag autocorrelation of CP-El Niño index of observations (black solid line), CESM1 model with snow radiative effect (CESM1-S: blue dashed line), and CESM1 model without snow radiative effect (CESM1-NOS: red dashed line).

Figure 7 shows the lead-lag autocorrelation coefficient of the CP-El Niño index for observations (black solid line), CESM1-S (blue dashed line), and CESM1-NoS (red dashed line) from a composite of CP-El Niño events. The NoS case shows higher autocorrelation (~0.3) that can be sustained up to 14 months before and after the event peak, relative to the observed and S cases. The longer and persistent composite CP-El Niño cycle is consistent with those found in SST and wind stress anomalies shown in Figures 5 and 6.

5. Summary and Discussion

All CMIP3 and most CMIP5 (28 out of 32) models only allow small particle cloud mass (i.e., suspended cloud ice particles) to interact with their radiative transfer codes and exclude the radiative effects of precipitation large particles, that is, falling snow. Previous work has identified long-term mean biases in cloud-radiation-dynamics interactions over the Pacific Ocean in CMIP5 models that are at least partly due to lacking precipitating ice

radiative effects (e.g., Li et al., 2013; Li, Lee, Waliser, David Neelin, et al., 2014; Li, Lee, Waliser, Stachnik, et al., 2014; Li et al., 2015, 2016). In particular, in convective regions, excluding falling-snow radiative effects in CESM1 boosts upper-level longwave radiative cooling and surface downward shortwave heating, leading to a radiative destabilization of the atmosphere that is excessively compensated by convective condensational heating. The deep cumulus parameterization responds with excessive cumulus updraft at higher levels (approximately $250 < P < 650$ hPa) and low-level downdraft as illustrated by Figure S4.

As a result, low-level moist and warm air originating from convective regions, which in the mean state are the warm pool and the ITCZ/SPCZ, is advected northeastward and southeastward. This weakens surface wind stress and reduces upper-ocean mixing, causing warmer SSTs (Figures 1 and 2) in the south central Pacific throughout the mean seasonal cycle.

This study examines the impacts of including snow radiative effects in a GCM on cloud-radiation and dynamics and shows how these effects modify simulated CP-El Niño behavior. When CP-El Niño occurs, convection is enhanced in the central Pacific and in the NoS case, the radiative instability and enhanced downdrafts have the effect of slowing the easterlies heading into the region, leading to SST warming and slowing the redevelopment of the cold tongue. In the S case, the lower-level divergence is relatively weaker and the associated stronger easterly winds keep the SSTs lower on the east side compared to NoS case. Unfortunately, the short QuikSCAT record does not capture enough CP-El Niño events to allow a rigorous analysis of the wind stress fields, but the model-observation discrepancy in SST propagation is much reduced in CESM1 when snow effects are included, in a way that is consistent with our proposed mechanism.

The exact manifestation of this process may be model dependent: first, because the vertical profile of snow within a model will affect heating rates, atmospheric stability, and low-level convective outflow, changing the magnitude of the S-NoS effect. Second, the ease with which CP-El Niño positive SST anomalies propagate eastward may depend on the strength of the mean state trade winds, which are affected by other processes. Indeed, CESM1 does not perfectly represent observed large-particle ice profiles reported in CloudSat-based products, it simply has much reduced biases once snow is included. However, given that the CESM1 results support our proposed mechanism and that any model's CP-El Niño event should include convective development in similar regions, our proposed process should occur in these models. We compared some properties between CMIP5-S and CMIP5-NoS models, but it is not possible to make a robust quantitative statement about snow radiative effects across the full ensemble since this comparison conflates all intermodel differences, not just snow radiative effects. Our results show that falling-snow radiative effects within CESM1 affect CP-El Niño events in a manner consistent with our proposed mechanism.

In this study we found reduced model-observation discrepancy in SST patterns not only in the west equatorial Pacific but also improved agreement on the east side of CP-El Niño warm anomalies. The unique feature of the CP-El Niño is the lack of East Pacific warming, and the spatial structure of temperature anomalies interacts with dynamics and the hydrological cycle. Similarly, by improving the mean state simulation as in CESM1-S, you will also improve precipitation location, dynamics, and the resulting teleconnections that can be important issues with ENSO and GCMs. The results were shown to be relatively consistent with other GCMs with snow interactions, so it would be useful if other GCMs began to include them as well to confirm the impacts. Teleconnection issues associated with El Niño events remain big challenges in GCMs. Overall, our CESM1 results are consistent with our proposed mechanism of a radiation-driven dynamical response to snow radiative effects which counteract several known biases across the CMIP5-NoS ensemble, so are strongly suggestive that including falling snow radiative effects in GCMs is important to improve the simulation of the Pacific mean state, seasonal cycle, and CP-El Niño. Further experiments with other GCMs would be necessary to better quantify these conclusions.

Acknowledgments
The contribution by J.-L L. to this study was carried out on behalf of the Jet Propulsion Laboratory, California Institute of Technology, under contracts of CCST, NDOA, and MEaSUREs programs with the National Aeronautics and Space Administration (NASA). The extended reconstructed sea surface temperature (ERSST: http://www.ncdc.noaa.gov/ersst/) analysis v3b (Smith et al., 2008) is used. The most up-to-date radiative data are available from the CERES Energy Balanced and Filled (EBAF) product (Loeb et al., 2009, 2012). The data can be found at http://ceres.larc.nasa.gov/order_data.php. The dynamical fields are from the European Centre for Medium-Range Forecasts (ECMWF) and can be downloaded at http://www.ecmwf.int/products/data/archive/descriptions/ei/.

References

Ashok, K., Behera, S., Rao, A. S., Weng, H., & Yamagata, T. (2007). El Niño Modoki and its teleconnection. *Journal of Geophysical Research*, *112*, C11007. https://doi.org/10.1029/2006JC003798

Collins, M., An, S. I., Cai, W., Ganachaud, A., Guilyardi, E., Jin, F. F., … Wittenberg, A. (2010). The impact of global warming on the tropical Pacific ocean and El Niño. *Nature Geoscience*, *3*(6), 391–397. https://doi.org/10.1038/ngeo868

Dee, D. P., & Uppala, S. (2009). Variational bias correction of satellite radiance data in the ERA-Interim reanalysis. *Quarterly Journal of the Royal Meteorological Society*, *135*(644), 1830–1841. https://doi.org/10.1002/qj.493

Ding, Q., Steig, E. J., Battisti, D. S., & Küttel, M. (2011). Winter warming in West Antarctica caused by central tropical Pacific warming. *Nature Geoscience*, *4*(6), 398–403. https://doi.org/10.1038/ngeo1129

Gettelman, A., Liu, X., Ghan, S. J., Morrison, H., Park, S., Conley, A. J., … Li, J.-L. F. (2010). Global simulations of ice nucleation and ice supersaturation with an improved cloud scheme in the Community Atmosphere Model. *Journal of Geophysical Research*, *115*, D18216. https://doi.org/10.1029/2009JD013797

Gettelman, A., Morrison, H., & Ghan, S. J. (2008). A new two-moment bulk stratiform cloud microphysics scheme in the Community Atmosphere Model, Version 3 (CAM3). Part II: Single-column and global results. *Journal of Climate*, *21*, 3660–3679. https://doi.org/10.1175/2008JCLI2116.1

Guilyardi, E., Wittenberg, A., Fedorov, A., Collins, M., Wang, C., Capotondi, A., … Stockdale, T. (2009). Understanding El Niño in ocean–atmosphere general circulation models: Progress and challenges. *Bulletin of the American Meteorological Society*, *90*(3), 325–340. https://doi.org/10.1175/2008BAMS2387.1

Ham, Y.-G., & Kug, J.-S. (2011). How well do current climate models simulate two types of El Niño? *Climate Dynamics*, *39*(1-2), 383–398. https://doi.org/10.1007/s00382-011-1157-3

Ham, Y.-G., Kug, J.-S., Kim, D., Kim, Y.-H., & Kim, D.-H. (2012). What controls phase-locking of ENSO to boreal winter in coupled GCMs? *Climate Dynamics*, *40*(5-6), 1551–1568. https://doi.org/10.1007/s00382-012-1420-2

Houze, R. A. Jr. (1997). Stratiform precipitation in regions of convection: A meteorological paradox? *Bulletin of the American Meteorological Society*, *78*(10), 2179–2196. https://doi.org/10.1175/1520-0477(1997)078%3C2179:SPIROC%3E2.0.CO;2

Kao, H.-Y., & Yu, J.-Y. (2009). Contrasting eastern-Pacific and central-Pacific types of El Niño. *Journal of Climate*, *22*(3), 615–632. https://doi.org/10.1175/2008JCLI2309.1

Kim, H.-M., Webster, P. J., & Curry, J. A. (2009). Impact of shifting patterns of Pacific Ocean warming on North Atlantic tropical cyclones. *Science*, *325*(5936), 77–80. https://doi.org/10.1126/science.1174062

Kim, S. T., & Yu, J.-Y. (2012). The Two Types of ENSO in CMIP5 Models. *Geophysical Research Letters*, *39*, L11704. https://doi.org/10.1029/2012GL052006

Kim, S. T., Yu, J.-Y., Kumar, A., & Wang, H. (2012). Examination of the two types of ENSO in the NCEP CFS model and its extratropical associations. *Monthly Weather Review*, *140*(6), 1908–1923. https://doi.org/10.1175/MWR-D-11-00300.1

Kug, J.-S., Jin, F.-F., & An, S.-I. (2009). Two types of El Niño events: Cold tongue El Niño and warm pool El Niño. *Journal of Climate*, *22*(6), 1499–1515. https://doi.org/10.1175/2008JCLI2624.1

Larkin, N. K., & Harrison, D. E. (2005). On the definition of El Niño and associated seasonal average U.S. weather anomalies. *Geophysical Research Letters*, *32*, L13705. https://doi.org/10.1029/2005GL022738

Lee, T., & McPhaden, M. J. (2010). Increasing intensity of El Niño in the central-equatorial Pacific. *Geophysical Research Letters*, *37*, L14603. https://doi.org/10.1029/2010GL044007

Lee, T., Waliser, D. E., Li, J.-L., Landerer, F. W., & Gierach, M. M. (2013). Evaluation of CMIP3 and CMIP5 wind stress climatology using satellite measurements and atmospheric reanalysis products. *Journal of Climate*, *26*(16), 5810–5826. https://doi.org/10.1175/JCLI-D-12-00591.1

Li, G., Ren, B., Yang, C., & Zheng, J. (2010). Indices of El Niño and El Niño Modoki: An improved El Niño Modoki index. *Advances in Atmospheric Sciences*, *27*(5), 1210–1220. https://doi.org/10.1007/s00376-010-9173-5

Li, J.-L. F., Lee, W.-L., Lee, T., Fetzer, E., & Yu, J.-Y. (2015). The impacts of cloud snow radiative effects on Pacific Oceans surface heat fluxes, surface wind stress, and ocean temperatures in coupled GCM simulations. *Journal of Geophysical Research: Atmospheres*, *120*, 2242–2260. https://doi.org/10.1002/2014JD022538

Li, J.-L. F., Lee, W.-L., Waliser, D. E., David Neelin, J., Stachnik, J. P., & Lee, T. (2014). Cloud-precipitation-radiation-dynamics interaction in global climate models: A snow and radiation interaction sensitivity experiment. *Journal of Geophysical Research: Atmospheres*, *119*, 3809–3824. https://doi.org/10.1002/2013JD021038

Li, J.-L. F., Lee, W.-L., Waliser, D. E., Stachnik, J. P., Fetzer, E., Wong, S., & Yue, Q. (2014). Characterizing tropical Pacific water vapor and radiative biases in CMIP5 GCMs: Observation-based analyses and a snow and radiation interaction sensitivity experiment. *Journal of Geophysical Research: Atmospheres*, *119*, 10,981–10,995. https://doi.org/10.1002/2014JD021924

Li, J.-L. F., Waliser, D. E., Chen, W.-T., Guan, B., Kubar, T., Stephens, G., … Horowitz, L. (2012). An observationally-based evaluation of cloud ice water in CMIP3 and CMIP5 GCMs and contemporary analyses. *Journal of Geophysical Research*, *117*, D16105. https://doi.org/10.1029/2012JD017640

Li, J.-L. F., Waliser, D. E., Stephens, G., Lee, S., L'Ecuyer, T., Kato, S., … Ma, H.-Y. (2013). Characterizing and understanding radiation budget biases in CMIP3/CMIP5 GCMs, contemporary GCM, and reanalysis. *Journal of Geophysical Research: Atmospheres*, *118*, 8166–8184. https://doi.org/10.1002/jgrd.50378

Li, J.-L. F., Wang, Y.-H., Lee, T., Waliser, D., Lee, W.-L., Yu, J.-Y., … Hasson, A. (2016). The impacts of precipitating cloud radiative effects on ocean surface evaporation, precipitation, and ocean salinity in coupled GCM simulations. *Journal of Geophysical Research: Atmospheres*, *121*, 9474–9491. https://doi.org/10.1002/2016JD024911

Lindvall, J., Svensson, G., & Hannay, C. (2013). Evaluation of near-surface parameters in the two versions of the atmospheric model in CESM1 using flux station observations. *Journal of Climate*, *26*(1), 26–44. https://doi.org/10.1175/JCLI-D-12-00020.1

Loeb, N. G., Lyman, J. M., Johnson, G. C., Allan, R. P., Doelling, D. R., Wong, T., … Stephens, G. L. (2012). Observed changes in top-of-the-atmosphere radiation and upper-ocean heating consistent within uncertainty. *Nature Geoscience*, *5*(2), 110–113. https://doi.org/10.1038/NGEO1375

Loeb, N. G., Wielicki, B. A., Doelling, D. R., Smith, G. L., Keyes, D. F., Kato, S., … Wong, T. (2009). Toward optimal closure of the Earth's top-of-atmosphere radiation budget. *Journal of Climate*, *22*(3), 748–766. https://doi.org/10.1175/2008JCLI2637.1

McPhaden, M. J., Zebiak, S. E., & Glantz, M. H. (2006). ENSO as an integrating concept in earth science. *Science*, *314*, 1739–1745.

Meehl, G. A., Stocker, T. F., Collins, W. D., Friedlingstein, P., Gaye, A. T., Gregory, J. M., … Zhao, Z.-C. (2007). Global climate projections. In S. Solomon, et al. (Eds.), *Climate change 2007: The physical science basis. Contribution of working group I to the fourth assessment report of the intergovernmental panel on climate change*. Cambridge, United Kingdom and New York: Cambridge University Press.

Mo, K. C. (2010). Interdecadal modulation of the impact of ENSO on precipitation and temperature over the United States. *Journal of Climate*, *23*(13), 3639–3656. https://doi.org/10.1175/2010JCLI3553.1

Morrison, H., & Gettelman, A. (2008). A new two-moment bulk stratiform cloud microphysics scheme in the Community Atmosphere Model, Version 3 (CAM3). Part I: Description and numerical tests. *Journal of Climate*, *21*(15), 3642–3659. https://doi.org/10.1175/2008JCLI2105.1

Neale, R. B., Gettelman, A., Park, S., Conley, A. J., Kinnison, D., Marsh, D., … Rasch, P. J. (2012). Description of the NCAR Community Atmosphere Model: CAM 5.0 (Tech. Rep. NCAR/TN-486+STR). National Center for Atmospheric Research, Boulder, CO.

Risien, C. M., & Chelton, D. B. (2008). A global climatology of surfacewind and wind stress fields from eight years of QuikSCAT scatterometerdata. *Journal of Physical Oceanography*, *38*, 2379–2413. https://doi.org/10.1175/2008JPO3881.1

Smith, T. M., Reynolds, R. W., Peterson, T. C., & Lawrimore, J. (2008). Improvements to NOAA's historical merged land–ocean surface temperature analysis (1880–2006). *Journal of Climate*, *21*(10), 2283–2296. https://doi.org/10.1175/2007JCLI2100.1

Taylor, K. E., Stouffer, R. J., & Meehl, G. A. (2012). An overview of CMIP5 and the experiment design. *Bulletin of the American Meteorological Society*, *93*(4), 485–498. https://doi.org/10.1175/BAMS-D-11-00094.1

Trenberth, K., & Stepaniak, D. P. (2001). Indices of El Niño evolution. *Journal of Climate*, *14*(8), 1697–1701. https://doi.org/10.1175/1520-0442(2001)014%3C1697:LIOENO%3E2.0.CO;2

Vecchi, G. A., & Wittenberg, A. T. (2010). El Niño and our future climate: Where do we stand? *WIREs Climate Change*, *1*, 260–270. https://doi.org/10.1002/wcc.33

Wang, C., & Weisberg, R. H. (2000). The 1997–98 El Niño evolution relative to previous El Niño events. *Journal of Climate*, *13*(2), 488–501. https://doi.org/10.1175/15200442(2000)013%3C0488:TENOER%3E2.0.CO;2

Wittenberg, A. T. (2009). Are historical records sufficient to constrain ENSO simulations? *Geophysical Research Letters*, *36*, L12702. https://doi.org/10.1029/2009GL038710

Yu, J.-Y., & Kao, H.-Y. (2007). Decadal changes of ENSO persistence barrier in SST and ocean heat content indices: 1958–2001. *Journal of Geophysical Research*, *112*, D13106. https://doi.org/10.1029/2006JD007654

Yu, J.-Y., Kao, H. Y., Lee, T., & Kim, S. T. (2011). Subsurface ocean temperature indices for Central-Pacific and Eastern-Pacific types of El Niño and La Niña events. *Theoretical and Applied Climatology*, *103*(3-4), 337–344. https://doi.org/10.1007/s00704-010-0307-6

Yu, J.-Y., & Kim, S. T. (2010). Identification of central-Pacific and eastern-Pacific types of El Niño in CMIP3 models. *Geophysical Research Letters*, *37*, L15705. https://doi.org/10.1029/2010GL044082